Cerebral Cortex February 2012;22:426–435
doi:10.1093/cercor/bhr121
Advance Access publication June 13, 2011

Noradrenergic Neurons of the Locus Coeruleus Are Phase Locked to Cortical Up-Down States during Sleep

Oxana Eschenko[1], Cesare Magri[1], Stefano Panzeri[2] and Susan J. Sara[3]

[1]Department of Physiology of Cognitive Processes, Max Planck Institute for Biological Cybernetics, 72076 Tübingen, Germany, [2]Department of Robotics, Brain and Cognitive Sciences, Italian Institute of Technology, 16163 Genova, Italy and [3]Laboratory of Physiology of Perception and Action, CNRS UMR 7192, Collège de France, F-75005 Paris, France

Address correspondence to Susan J. Sara, Collège de France, CNRS, UMR 7152, F-75005 Paris, France. Email: susan.sara@college-de-france.fr.

Nonrapid eye movement (NREM) sleep is characterized by periodic changes in cortical excitability that are reflected in the electroencephalography (EEG) as high-amplitude slow oscillations, indicative of cortical Up/Down states. These slow oscillations are thought to be involved in NREM sleep-dependent memory consolidation. Although the locus coeruleus (LC) noradrenergic system is known to play a role in off-line memory consolidation (that may occur during NREM sleep), cortico–coerulear interactions during NREM sleep have not yet been studied in detail. Here, we investigated the timing of LC spikes as a function of sleep-associated slow oscillations. Cortical EEG was monitored, along with activity of LC neurons recorded extracellularly, in nonanesthetized naturally sleeping rats. LC spike-triggered averaging of EEG, together with phase-locking analysis, revealed preferential firing of LC neurons along the ascending edge of the EEG slow oscillation, correlating with Down-to-Up state transition. LC neurons were locked best when spikes were shifted forward ~50 ms in time with respect to the EEG slow oscillation. These results suggest that during NREM sleep, firing of LC neurons may contribute to the rising phase of the EEG slow wave by providing a neuromodulatory input that increases cortical excitability, thereby promoting plasticity within these circuits.

Keywords: locus coeruleus, memory consolidation, neuromodulation, noradrenergic system, prefrontal cortex, sleep, slow oscillations

Introduction

Recent years have seen a growing interest in the role of sleep in off-line memory processing (Stickgold 2005; Diekelmann and Born 2010). This interest is due, in part, to the discovery of large-scale changes in cortical and hippocampal neural activity during nonrapid eye movement (NREM) sleep following learning. Learning-related enhanced spindle and ripple activity has been reported in both humans (Gais et al. 2002; Schabus et al. 2004; Clemens et al. 2006; Axmacher et al. 2008; Morin et al. 2008) and rats (Eschenko et al. 2006, 2008; Fogel and Smith 2006; O'Neill et al. 2008; Ramadan et al. 2009). During sleep, the membrane potential of all major types of neocortical neurons fluctuates between depolarized (Up) and hyperpolarized (Down) states; the transitions between these states are reflected in electroencephalography (EEG) as large-amplitude, low-frequency (~1 Hz) slow waves (Steriade et al. 1993a, 1993b; Steriade et al. 2001; Timofeev et al. 2001). Slow oscillations group the faster brain rhythms, spindles in the cortex (Mölle et al. 2002; Steriade 2006), and ripples in the hippocampus (Siapas and Wilson 1998; Sirota et al. 2003; Mölle et al. 2006). In turn, these fast transient oscillations reflect synchronized firing of large neuronal populations during the depolarized state, including the well-documented experience-dependent neuronal replay in cortex and hippocampus (Kudrimoti et al. 1999; Nadasdy et al. 1999; Johnson et al. 2010). Thus, the slow oscillations are thought to mediate sleep-dependent memory improvements by temporally coordinating other brain rhythms implicated in off-line information processing (Steriade and Timofeev 2003; Diekelmann and Born 2010). Such concerted brain activity may reinforce the neuronal networks being replayed by facilitating communication within and between brain regions and promoting synaptic plasticity (Buzsaki 1996).

The noradrenergic (NE) system has been shown to be critically involved in the late phase of memory consolidation (Roullet and Sara 1998; Tronel et al. 2004) that may well take place during NREM sleep. In support of this notion, we previously described a transient increase in activity of NE neurons of the locus coeruleus (LC) during NREM sleep after learning in rats (Eschenko and Sara 2008). A combined EEG and functional magnetic resonance imaging (fMRI) study in humans (Dang-Vu et al. 2008) further revealed that the activity of the LC nucleus is temporally related to slow oscillations. Altogether, these findings challenge the conventional dogma about the relative quiescence of LC neurons during sleep (Hobson et al. 1975; Aston-Jones and Bloom 1981) and suggest an involvement of LC-NE system in modulating cortical activity during NREM sleep.

Although the facilitating effects of the LC input on cortical excitability (McCormick et al. 1991), spike timing and synaptic plasticity in cortex (Bouret and Sara 2002; Marzo et al. 2009), and hippocampus (Harley 2007) are well established, the precise temporal relationship between cortical Up/Down states and LC firing has not yet been explored. Our previous investigations in rats under ketamine anesthesia had shown a negative correlation in activity of NE neurons of the LC and prefrontal neurons, when neurons within each region were oscillating at ~1 Hz (Sara and Herve-Minvielle 1995; Lestienne et al. 1997). Therefore, in order to further explore the fine-scale temporal cortico–coerulear interaction, particularly in the context of potential contribution of the LC-NE system to memory processing during NREM sleep, we recorded unit activity in the LC simultaneously with cortical EEG in the unanaesthetized naturally sleeping rat.

Materials and Methods

Animals

Male Sprague–Dawley rats (Charles River Laboratories, Le Genest-St-Isle, France), weighing 350–400 g were used. They were maintained on a 12:12 h light:dark cycle with free access to food and water. Surgery was performed under pentobarbital anesthesia (40 mg/kg, supplemented as necessary). Rats were allowed 1 week for postsurgical recovery, before being habituated to the recording setup. All procedures followed the 1986 European Community Council Directive

and the French Ministère de l'Agriculture et de la Foret, Commission Nationale de l'Experimentation Animal decree 87848.

Electrophysiological Recordings

For extracellular recording, 2 tungsten electrodes (~1 MΩ; FHC, Bowdoinham), glued together (200–500 μm between the tips), and mounted on a movable microdrive, were implanted in the LC region in 5 rats (Anterior-posterior [AP] = –4.0 mm, L = 1.15 mm) under electrophysiological control. One electrode served as a reference for differential recording, with care being taken that the unit activity was coming from only one electrode. This method eliminates muscle artifacts picked up in freely moving animals, especially when the electrodes are located deep in the brain stem; the method has been used extensively in our laboratory (Sara and Segal 1991; Bouret and Sara 2004; Eschenko and Sara 2008). For EEG recording, a stainless steel screw was secured on the skull in all rats above the frontal cortex (Bregma: AP: 2–4 mm, L: 0.5 mm). EEG was referenced to a skull screw above the cerebellum.

Rats were connected to the recording system via a rotating cable allowing free movement within the recording box (25 × 25 × 50 cm). Recordings were made for 3–5 h during the light period, when rats spend most of their time sleeping. For unit recording, extracellular signals were amplified (×10 k) and filtered (300–6 kHz) using a differential amplifier (A-M Systems model 1700, Inc., Carlsborg, WA). EEG signal was amplified (×1 k) and filtered (0.1–300 Hz). The unit and EEG signals were digitized at 32 kHz and 2 kHz, respectively, using CED Power1401 converter and Spike2 data acquisition software (Cambridge Electronic Design, Cambridge, UK). A video camera (Quickcam, Logitech, Switzerland) was mounted on the top of the recording chamber, the image synchronized with electrophysiological recording.

Unit activity was monitored online, and spikes with signal-to-noise ratio greater than 2:1 were used to create templates using Spike2 software. The following additional criteria were applied for identification of LC neurons: 1) broad spike widths (~0.6 ms); 2) regular low firing rate (1–2/s) during the quiet awake state; 3) a brief excitation to acoustic stimuli followed by prolonged inhibition, and 4) REM-silence, which was verified offline (Hobson et al. 1975; Foote et al. 1980; Aston-Jones and Bloom 1981; Sara and Segal 1991; Herve-Minvielle and Sara 1995). Characteristic features of the LC neurons and the electrode placement are illustrated on Supplementary Figure 1. If the unit discharge did not meet these criteria, the electrode was lowered by 40 μm increments to reach a reliable LC signal. In 4 additional rats, several recordings were made of unit activity that was clearly not characteristic of LC neurons. These were used as control data. The electrode placement for these control cases is illustrated in Supplementary Figure 2.

Fifteen additional recordings were obtained from the medial prefrontal cortex (mPFC) in 5 rats. These data were originally collected for another study and published in detail elsewhere (Mölle et al. 2006). We used the same differential recording method described above for LC, with 2 microelectrodes mounted on a moveable microdrive and implanted in the mPFC at the following coordinates (Bregma: AP = 3.5 mm, L = 0.5 mm). The depth was adjusted within a range of 3–4 mm from the brain surface at the time of recording, in order to obtain an optimal signal. In 2 rats, local field potentials (LFPs) were also recorded from the same electrode tip. It is important to emphasize that the mPFC and LC recordings were made using the same recording technique, in the same recording setup, and in the same behavioral situation. The placement of the EEG electrodes was identical in the 2 experimental groups. Finally, the same spike sorting algorithms were applied for all data sets by the same investigator (O.E.).

Signal Processing and Event Detection

Unit Isolation

After online detection, the stored spike shapes were further isolated from electrical noise offline with template matching complemented by cluster analysis based on principal components and specific wave form measurements, using Spike2 software. A representative example of the isolated LC spike shapes is shown on Supplementary Figure 1*B*. The recording technique and spike sorting method did not allow an unambiguous single unit isolation, and therefore, the LC, non-LC, and mPFC unit recordings described in the present study are conservatively classified as multiunit activity. It should be noted, however, that the overestimation of activity by inclusion of noisy spikes can only decrease the statistical power for detecting locking to slow waves and cannot artificially create locking that does not exist. Therefore, our estimates can be taken as credible lower bounds to the actual amount of locking.

Sleep Scoring

NREM sleep episodes were detected by the presence of a high-amplitude slow activity (>200 μV), predominance of delta (1–4 Hz), and absence of theta (6–9 Hz) frequencies in the power spectrum and regular appearance of sleep spindles in the EEG. To identify the sleep spindles, the EEG signal was band-pass filtered using finite impulse response (FIR) of 12–15 Hz; an automatic spindle detection algorithm was then applied (Eschenko et al. 2006). REM sleep was characterized by dominant theta activity, low-voltage fast activity, and a sleep posture monitored by online video recording. A representative pattern of EEG and LC activity across awake/sleep stages is illustrated on Supplementary Figure 1*D*.

Detection of Slow Oscillations

A high-pass filter in the majority of analog amplifiers designed for extracellular recording (including the one used in the present study) introduces a systematic frequency-dependent phase shift that is appreciable for low frequencies. We corrected for this phase delay by filtering the EEG signal backward in time using a second-order Butterworth low-pass filter with a cutoff frequency of 0.11 Hz. The order of the filter was determined from the technical specifications of the amplifier while the cutoff frequency was selected after inspecting the output of the amplifier to controlled inputs. This procedure, which is detailed fully in Supplementary Methods and illustrated on Supplementary Figure 3, enabled a more accurate detection of the timing of slow oscillation events and a precise determination of their phase.

Slow oscillation cycles were then identified by peaks of negativity of the EEG signal during NREM sleep episodes, as follows. The EEG signal was first low-pass filtered using FIR of 4 Hz. Then, the largest negative half-waves during NREM sleep episodes were detected using a standard algorithm (Mölle et al. 2002). Negative half-waves satisfying the following criteria were selected for further analyses: 1) 2 successive zero-crossings of the low-pass filtered signal separated from each other by at least 0.2 s; 2) maximum amplitude between both zero-crossings exceeding –100 μV; and 3) a negative-to-positive peak-to-peak amplitude >120 μV. Validity of this algorithm for detection of cortical Up and Down states using EEG was previously assessed by calculation of an event correlogram for prefrontal units around the negative peaks of slow oscillations (Mölle et al. 2006). Peak negativity is considered to reflect the transition of the intracellulary recorded membrane potential to the depolarizing phase (Steriade et al. 1993a, 1993b; Volgushev et al. 2006; Saleem et al. 2010).

Normalized Autocorrelogram

The normalized autocorrelograms were computed by first binning spike trains into 50-ms bins and then computing the covariance between the spike train and its time-shifted version. In order to facilitate comparison between data sets with different overall spike numbers, the obtained autocorrelograms were normalized by dividing by total number of spikes used for the computation.

Event-Triggered Analysis

We computed the firing rate in a window centered around the negative peak of the detected slow oscillations cycle and extending 0.75 s each side with the bin size of 20 ms. For each session, we normalized the firing rate in each bin to the total number of spikes (collected across all detected events) within the analysis window of ±0.75 s. We also computed (using the same bin size) the baseline rate in the 0.75-s interval preceding the window around the wave negativity. The same normalization as above was also applied to the baseline rate. To compare the distribution of the firing rate in each individual bin around the wave negativity, to the distribution of the firing rate in the baseline period, across sessions, we used a *t*-test with significance level set to $P = 0.01$ (2-tailed), Bonferroni corrected for the total number of bins considered.

Phase Analysis

Phase was assigned to each spike within a slow oscillation cycle as follows. First, 5 salient points in each detected slow oscillation were determined: slow oscillation onset (the positive-to-negative zero-crossing preceding the negative peak), peak negativity, the middle zero-crossing (negative-to-positive), the peak positivity, and the wave ending point (the positive-to-negative zero-crossing following the positive peak). These 5 points were assigned a fixed phase, as illustrated in Supplementary Figure 4. We computed the phase of the other points in the slow oscillation by linear interpolating between each of the 5 assigned phase values.

"Phase-of-firing distribution" is computed from the phase value at which each spike fires. Phase of firing not uniformly distributed over 360° reflects the fact that there are phase regions at which the considered neurons fire preferentially. This defines "phase locking" of spikes. The analysis of phase locking may be confounded by asymmetries in the waveforms where the overall distribution of phases is not uniform, making it difficult to establish that the probability of observing a spike significantly depends upon the phase value. To correct for this, we used a standard procedure based on rescaling phase, using its cumulative distribution (Fisher 1993; Siapas et al. 2005), and the schematic in Supplementary Figure 4. In this way, the overall distribution of phases, unconditioned to spike time, becomes uniform, and the question of phase locking detection is reduced to simply detecting departures from uniformity in the distribution of rescaled phases observed at spike times. The significance of the departure from phase uniformity can then be safely computed using the Rayleigh test, which is the standard test for significance of deviations of angular distribution from nonuniformity (Fisher 1993; Siapas et al. 2005).

Since maximal phase locking between spike train and slow wave need not occur when the 2 signals are aligned, units were labeled as "phase locked" whenever the Rayleigh test P value exceeded the significance threshold $P = 0.01$ at any value of the shift of the EEG trace with respect to the spike train within −1 and 1 s. The significance threshold $P = 0.01$ was Bonferroni corrected for the total number of shifts of the EEG trace considered. It is important to note that the method used here, which follows previous well-established work (Siapas et al. 2005; Montemurro et al. 2008), computes phase selectivity of the entire distribution of spikes emitted during slow waves. Therefore, the preferential phase of firing reflects the phase regions with the overall highest firing; the method cannot distinguish more detailed information such as the phase of onset or offset of certain types of precisely timed bursts of activity.

As a measure of "strength of locking," we used one minus the circular variance. Circular variance is the most widely used measure of angular dispersion (defined, e.g., Fisher 1993; Montemurro et al. 2008). Therefore, the strength of locking defined in this way is a measure of the concentration of the distribution of angles, and its values range from 0 (uniform dispersion of angles along the circle) to 1 (perfect concentration of angles around one phase value).

In order to validate the method and facilitate comparison between 2 brain regions, we performed similar phase-locking analysis for mPFC neurons. We have previously reported that all mPFC neurons from this data set preferentially fired ~90 ms prior to the peak of the depolarized state (Mölle et al. 2006).

Histology

Rats were deeply anesthetized with pentobarbital (100 mg/kg), perfused intracardially, and brains extracted for histological verification of the recording sites. Adjacent sections were stained with Cresyl Violet or immunohistochemically for tyrosine hydroxylase to label NE neurons. All recordings sites were verified histologically (Supplementary Figs 1 and 2).

Results

LC Firing Pattern

Thirty-three data sets recorded in 21 sessions from 5 rats satisfied the criteria for a LC neuron (see Materials and Methods and Supplementary Fig. 1). The range of recording sessions for an individual rat varied from 2 to 7 sessions. Before each recording session, the electrode position was adjusted within a range of 40–120 μm using the movable microdrive to obtain the best signal-to-noise ratio. The average firing rate of all recorded LC neurons during NREM sleep was 0.65 ± 0.02 spikes/s (mean ± standard error of the mean), significantly lower than that measured during the awake state (1.50 ± 0.05 spikes/s; $t_{64} = -5.9$; $P < 0.001$). Thus, the state-dependent firing rate of the majority of LC recordings was within a firing range previously reported for LC single units (Aston-Jones and Bloom 1981). Nevertheless, the recording and spike sorting methods used in these experiments do not always allow unambiguous determination of single-unit activity, so the records may contain more than one unit. Figure 1*A* illustrates a representative example of LC spiking activity during the transition from NREM sleep to awake. There was an increase in LC firing just prior to the transition from NREM sleep to awake state with corresponding changes in EEG from slow high-amplitude signal during NREM sleep, to the faster, low-amplitude EEG of the awake state. This anticipatory increase of LC activity is a characteristic feature of the LC neurons (Aston-Jones and Bloom 1981). The higher rate of firing is sustained across wakefulness. Despite substantially lower LC activity during NREM sleep, it was more synchronized compared with the awake state. LC neurons showed a clear tendency to fire in bursts during NREM sleep as illustrated in Figure 1*C*. The change in firing pattern is reflected in the multiunit normalized autocorrelogram showing higher firing value around zero lag during NREM sleep, compared with the awake state, where the normalized autocorrelogram is flatter (Fig. 1*C*).

Temporal Analysis of LC Firing as a Function of Slow Oscillation Cycle

LC units were recorded simultaneously with the frontal EEG that was used for detecting slow oscillation cycles (see Materials and Methods). The number of detected slow oscillation events ranged from 788 to 4341 per recording session. The average amplitude (negative peak amplitude) and width (time from the start to the end of the slow oscillation) of the detected slow oscillation cycles was 0.20 ± 0.01 mV and 0.65 ± 0.02 s, respectively.

To investigate temporal relations between LC firing and occurrence of cortical Up/Down states, LC spikes were plotted around negative peaks of detected slow oscillation cycles. When aligning LC spikes to the negative peak of the slow oscillation (Fig. 1*D*), it is apparent from this example that LC preferentially fired in the restricted time interval immediately following the peak negativity (Fig. 1*D*). The strong relationship between LC firing and slow oscillation cycles is further illustrated by the LC spike-triggered average EEG (Fig. 1*E*), which shows, for this example, that EEG negativity peaks precede LC spikes.

The population analysis of all LC data sets ($n = 33$, recorded in 5 rats) confirmed that LC firing rate varied significantly across the slow oscillation cycle. Distribution of LC firing rates at around the times of negative and positive peaks of slow oscillation cycles with corresponding average EEG signal is shown on Figure 2. Statistical analysis revealed that the averaged LC firing rate was significantly lower than baseline firing rate in the period 130–190 ms prior to the slow wave negativity and was significantly higher than baseline in the

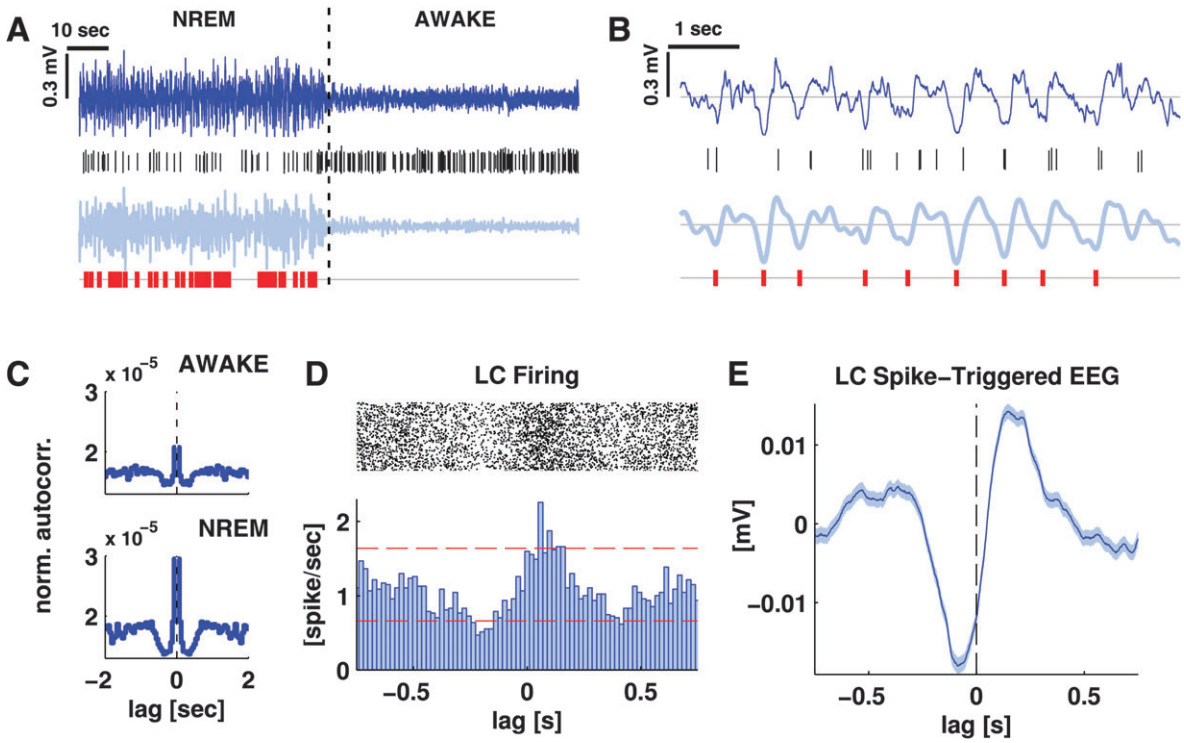

Figure 1. Firing activity of LC neurons during awake and NREM sleep. (*A*) Example of EEG (dark blue trace) and LC firing (black marks) recorded simultaneously during the transition from a NREM sleep period to a quiet awake state (each black mark represents an LC spike and the size of the mark reflects the spike amplitude). Cortical EEG was recorded above prefrontal cortex. The delta component (0.1–4 Hz) of EEG is shown (light blue trace). The red marks indicate the detected negative peaks of the slow oscillations. Note a characteristic increase in LC firing rate just preceding the change in EEG. (*B*) Expansion of the NREM sleep episode of the record shown in panel *A*, to illustrate the temporal relation between LC spikes and the slow oscillation cycle. Note, LC spikes preferentially occur after the negative peak (Down state) and before the positive peak (Up state). (*C*) Autocorrelogram of a representative LC recording during awake (top panel) and NREM sleep (bottom panel) with a resolution of 50 ms. The higher peak around zero during NREM sleep reflects the fact that the LC fires preferentially in a burst mode. Note that in this panel we did not plot the correlation at lag zero, which would go out of scale and is not of interest for this analysis. (*D*) Firing rate distribution around the peak negativity of the EEG slow oscillation. Each line in the raster plot shows the distribution of individual spikes across a slow oscillation cycle. Bars represent the average firing rate computed over all detected slow oscillations using 20-ms bins. Horizontal dashed lines show 99% confidence intervals. Note that LC firing decreases ~200 ms before the trough of the slow oscillation and increases immediately after. (*E*) Spike-triggered average of the nonfiltered EEG signal during NREM sleep episodes triggered on the LC spikes. Curves are plotted as average (solid line) and standard error of the mean (shaded area). Note that the LC fires immediately after the EEG slow wave peak negativity. Data from the same recording session are shown on all panels of Figure 1.

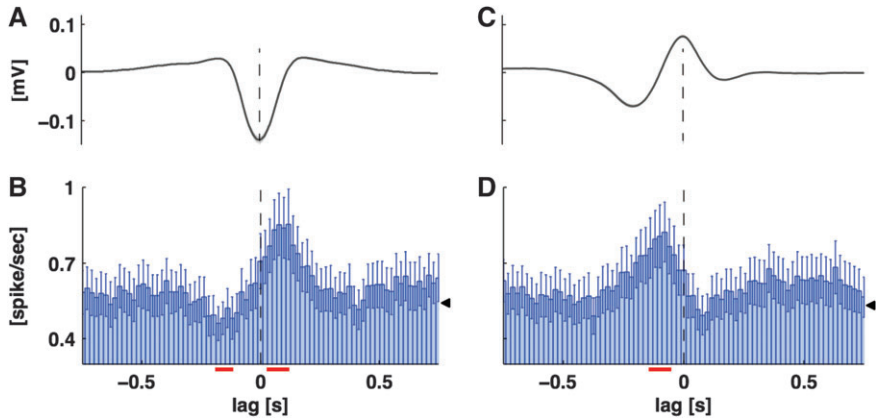

Figure 2. Temporal relationship between the LC firing activity and cortical Up and Down states. (*A*, *C*) Average of the nonfiltered EEG around the negative peak (panel *A*) and the positive peak (panel *C*) of the slow oscillation cycle. Peak negativities were detected from the delta (0.1–4 Hz) component of the EEG signal (for details, see Materials and Methods). (*B*, *D*) The LC firing rate around the peak negativity (panel *B*) and the peak positivity (panel *D*) of the slow oscillation cycle. The red segments show the time ranges in which LC firing is significantly different from baseline firing ($P < 0.05$ Bonferroni corrected; 2 sample 2 tails *t*-test). The population average of the LC baseline firing rate is indicated by a black triangle. Note the significant decrease in LC activity before the peak negativity and along the rising edge of the slow wave. All results are plotted as mean ± standard error of the mean across sessions. The bin size is 20 ms.

period 30–130 ms after the negative peak of detected slow oscillation cycles ($P < 0.01$; 2-tailed *t*-test Bonferroni corrected), as indicated in Figure 2*B*.

It should be noted that the slow oscillation cycles used in the above analysis were detected as high-amplitude (>120 μV) low-frequency (~1 Hz) EEG events (see Materials and Methods). To

determine whether the selection of the detected slow oscillation cycle was crucial for timing of LC firing, we analyzed the LC spike-triggered EEG during the time periods when a high-amplitude slow oscillation was detected and outside of the detected events. The shape of the LC spike-triggered EEG did not change much from one case to the other (Supplementary Fig. 5), suggesting that the locking of LC spiking activity to negativities of the EEG is largely independent of EEG amplitude.

Analysis of Phase of Firing during the Slow Oscillation Cycle

Each instance of a naturally occurring slow wave has a slightly different shape and duration (referred to as a slow wave microstructure). This introduces an additional variability factor when relating neural firing to slow oscillation cycles in the time domain. Phase analysis characterizes locking with respect to the salient properties of the slow waves (e.g., peaks and troughs), which are invariant with changes in wave shape and duration. Thus, it allows compensation for the differences in the microstructure of the slow wave. Consequently, it makes interbrain region or intersubject comparisons more accurate.

The phase relationship to the slow oscillation cycle was explored for each LC recording by estimating the probability of firing at different phases of the slow oscillation (see Materials and Methods). Such probability is illustrated for a representative example in Figure 3*A*. In this example, the probability of firing was significantly modulated as a function of the phase of the slow wave (Rayleigh test, $P < 0.001$) and had a unimodal phase-of-firing probability, with a preferred phase of 229°. Overall, the probability distribution of 17 of 33 LC data sets (52%) was significantly modulated by the phase of slow oscillation (Rayleigh test, $P < 0.001$). In 2 rats, all cases showed significant locking. The recordings in the remaining 3 rats contained both significantly locked and nonlocked units. The distribution of preferred phase for all significantly modulated LC units is shown on Figure 3*C*,*E*. The preferred phase was concentrated within the range of 200–300° (circular population mean 251°) (Fig. 3*C*), this range corresponding to the ascending (depolarizing) phase of the slow wave (Fig. 3*E*).

Fifteen data sets with combined EEG and mPFC unit activity (see Materials and Methods) were also submitted to phase analysis. In 2 rats, LFPs were also recorded from the same electrode tip. The phase-of-firing of a sample mPFC recording is shown in Figure 3*D*. All PFC neurons (15/15) showed a significant dependence of firing on the phase of slow oscillation in the EEG (Rayleigh test, $P < 0.001$). The distribution of preferred phase-of-firing of the mPFC population (Fig. 3*D*) was concentrated in the range 280–360° (circular population mean equal to 322 deg). Thus, LC and mPFC neurons show minimally overlapping intervals of the preferred phase-of-firing (Figs 3*C*,*D* and 4*D*). In general, LC spikes that displayed significant locking to the slow oscillation cycle tend to be emitted before the mPFC spikes.

Recent work has demonstrated that transitions to an Up state in neocortex are tightly predicted by a phase of low frequency (<2 Hz) cortical LFPs (Saleem et al. 2010). As we reported previously, the time of EEG peak negativity closely corresponds to the time of the LFP positive peaks (Mölle et al. 2006). In addition, EEG and LFP signals show a strong negative correlation with no time delay (Supplementary Fig. 6*A*). Taking into account that the polarity of EEG and LFP signals recorded in the deep cortical layers is reversed, the work of Saleem et al. (2010) implies that transitions to a depolarized state occur

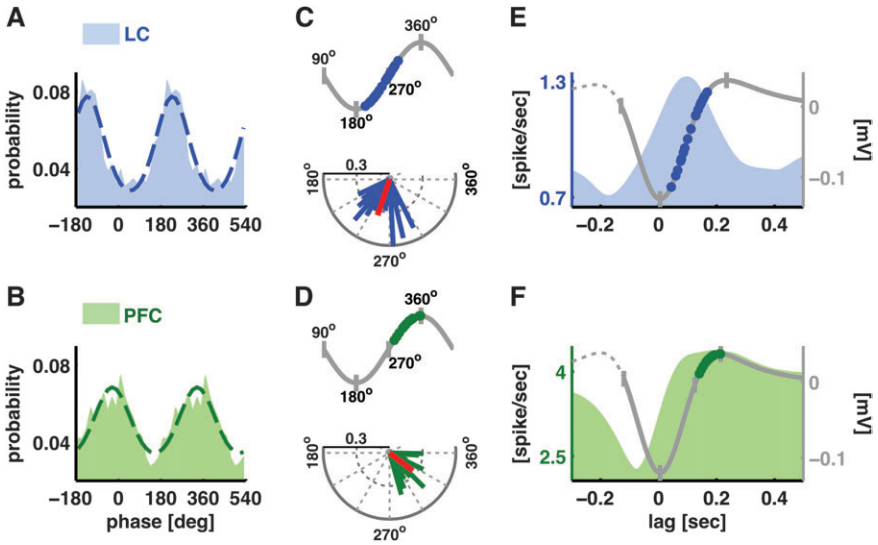

Figure 3. Preferred phase-of-firing of LC and PFC neurons. (*A*, *B*) Phase-of-firing distribution (colored area plot) with respect to the slow oscillation for a representative LC (*A*) and mPFC (*B*) case; 2 phase cycles are shown for clarity. The dashed line displays the fitted von Mises probability distribution. (*C*, *D*) Phase-of-firing distribution for all significantly phase-locked cases: 52% of LC and 100% of mPFC data sets. The gray sinusoidal wave is a schematic representation of an average slow oscillation after correcting for asymmetries (see Materials and Methods). The preferred phase-of-firing is marked as a colored dot for each case. The figure uses the following phase convention: 180 and 360° corresponding to the negative and positive peaks of the slow oscillation, respectively, 90° corresponding to the slow-wave start and 270° corresponding to the point of zero-crossing. In the polar plots, the phase and strength of locking are shown in the form of oriented bars: the orientation of each bar specifies, for each case, the preferred phase-of-firing while the length of the bar indicates the strength of locking. The red bar shows the population average. (*E*, *F*) The firing activity of LC and mPFC neurons relative to cortical Up/Down states. The area plot shows the smoothed time-dependent firing-rate of LC (*E*) and mPFC (*F*) neurons aligned to the peak negativity of the slow oscillation. The superimposed gray line shows the average EEG signal at the time of occurrence of the high-amplitude slow oscillation. In the figure, the slow wave negative peak is taken as the reference time $t = 0$. Dots indicate the preferred time of locking for LC (*E*) and PFC (*F*) neurons. Time of locking was computed from the preferred phase-of-firing values shown in Panel *C* and *D* by antitransforming the phase values into the time domain (see Materials and Methods).

(with our phase conventions) at 270° of the EEG slow wave. Overall, these results suggest that LC fires preferentially close to the time of transition to the Up state, while prefrontal neurons preferentially fire during the depolarized state, well after the Down-to-Up state transition.

LC and mPFC Neurons Are Maximally Locked to the Slow Oscillation at Different Temporal Offsets

In addition to establishing the statistical significance of phase locking, we further characterized the strength of locking in the 2 regions by computing the circular variance. To investigate the potential causal relationships in the observed phase locking, we computed the strength of phase locking as a function of the time shift τ between the detected slow oscillation and the LC or mPFC neuronal spike trains following Siapas et al. (2005), see Materials and Methods. Computing phase locking between time-shifted EEGs and LC spikes is of interest for several reasons, discussed in detail by Siapas et al. (2005). First, when no shift is applied, the maximal strength of locking is not always revealed (for an example, see Supplementary Discussion). Second, the time shift analysis helps to rule out the possibility that locking is merely due to intrinsic periodicities of the firing signals. Third, the shift analysis helps to establish a temporal order of the firing events that lock to the slow wave. Knowing the temporal order of events is, in turn, useful to identify which events are causes and which are effects.

The dependence of the strength of locking on the time shift, averaged separately over significantly phase-locked LC recordings (52%, 17/33) and mPFC neurons (100%, 15/15), is shown in Figure 4*A* (note that our convention is to report the lag τ by which we shifted the EEG trace). It is apparent that the neurons in both regions are only phase locked to slow waves for a time shift range of approximately 400 ms in either future or past. Therefore, the locking of PFC and LC neural activity to the slow oscillation cycle cannot be explained by some intrinsic periodicity of the spiking signals at roughly the same frequency. Naturally occurring high-amplitude slow waves are not constant in frequency but show a pattern of small frequency fluctuations over time. Because of such microstructure of slow waves, a neuron with rhythmic firing at a fixed frequency in the slow frequency (<2 Hz) range will not necessarily show phase locking. The results reported in Figure 4*A* show that both mPFC and LC neurons truly lock to the microstructure of the slow waves.

Finally, we compared the distribution of locking strength. These results are shown in Figure 4*D* both for the case of τ = 0 (no shifting between spikes and EEG) and for the τ value corresponding to the maximal locking of the population average. Figure 4 shows that the strength of locking was comparable in the 2 neuronal populations when only significantly locked cases were considered (52% and 100% for LC and mPFC neurons, respectively). For example, at time of maximal locking, the average locking strength was 0.16 ± 0.02 and 0.21 ± 0.02, for mPFC and LC, respectively (Fig. 4*B*). Thus, the major difference between the locking properties of the 2 brain regions lies in the proportion of modulated neurons (100% for PFC and ~50% for LC). The significantly modulated LC neurons were locked as strongly as the PFC neurons to the slow oscillation cycle recorded in the frontal EEG. As expected, a stronger locking to the slow waves was obtained for mPFC neurons when the slow waves were detected in the LFPs recorded from the same electrode tip. This reflects tighter relationships within a local cortical circuit (Supplementary Fig. 6*B*).

Figure 4*A* illustrates that, for both mPFC and LC neurons, the maximal locking was reached at negative time shifts τ (τ < 0 means EEG slow wave shifted back in time with respect to the spike train). Since the distribution of τ_{max} was non-Gaussian, nonparametric statistics were used for further analyses. Prefrontal spikes were maximally locked to the slow waves shifted back in time with a median delay τ_{max} of –105 ms (interquartile range –140 to –51 ms). The median delay $\bar{\tau}_{max}$ of the mPFC population was significantly different from zero (Wilcoxon signed-rank test; $P < 0.001$; Fig. 4*C*). This confirms that prefrontal neuronal activity contributes preferentially to the part of the slow wave around its peak that corresponds to a period of maximal cortical excitability. The maximal phase locking of the LC spikes occurred at time delays which were significantly negative (Wilcoxon signed-rank test; $P < 0.05$), although at a significantly shorter delay (Wilcoxon rank sum test; $P < 0.05$) than that of mPFC spikes. The median time offset of maximum locking of LC spikes was $\bar{\tau}_{max}$ = –50 ms (interquartile range –96 to 8 ms). The fact that LC neurons

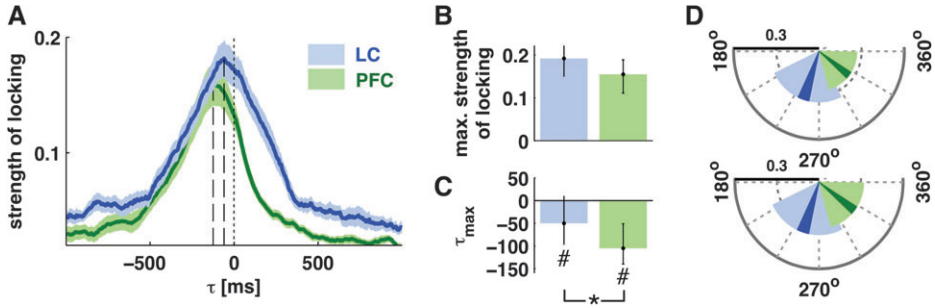

Figure 4. Strength of locking to the slow oscillation. (*A*) Strength of locking of LC and mPFC spikes to the slow oscillations for different values of the offset τ by which the slow oscillation cycle was shifted with respect to the spike train (see Materials and Methods). Curves are plotted as average (solid line) and standard error of the mean (shaded area) across the population. Only significantly phase-locked cases (52% of LC units and 100% of PFC data sets) are considered. Note that the strength of locking is comparable in the 2 brain regions. (*B*, *C*) Bars represent the population median (with error bars indicating interquartile range) of the maximal strength of locking (*B*) and the offsets τ_{max} at which the maxima occurred (*C*). Note the τ_{max} for both LC and mPFC neurons was negative and significantly different from zero. (*D*) The angular areas in the polar plots show the distribution of the preferred phase-of-firing angles for LC (blue) and PFC (green). Light colors are used to indicate the whole (min-to-max) range. Darker areas show the standard error of the mean. Note the almost nonoverlapping LC and mPFC phase-locking regions. The radius of the angular segments indicates the strength of locking. The top plot shows the locking at $\tau = 0$ and the bottom plot shows the locking at τ corresponding to the maximal strength of locking of the population average. * = $P < 0.05$ for between-group comparison, # = $P < 0.05$ for significant difference from zero.

are maximally locked to the EEG slow wave shifted a few tens of milliseconds back in time is consistent with the interpretation that LC spikes influence the ascending edge of EEG slow wave.

Specificity of the LC Locking to Cortical Slow Oscillations

We also analyzed the data sets obtained from 4 rats with recording in brain stem structures adjacent to the LC nucleus. The electrode placements for these cases are illustrated in Supplementary Figure 2. Histological examination of the recording sites showed that in one rat the electrode track was medial to LC in close proximity to the posteriordorsal tegmental nucleus (PDTg, $n = 4$ cases). In the second rat, the recordings sites were anterior to LC ($n = 10$ cases), some of them most likely corresponding to the laterodorsal tegmental nucleus (LDTg). Recordings from the third rat were obtained from the medial vestibular nucleus (MVe, $n = 4$), which is located posterior to LC. In the fourth rat, recording were obtained ventrally to the LC in subcoeruleus region ($n = 9$ cases). Some neurons located ventral to LC expressed robust firing during REM sleep and were essentially silent during NREM sleep ($n = 8$) and thus could not be subjected to the phase analysis. None of the neurons recorded in 4 brain areas adjacent to LC ($n = 19$ cases) showed a sign of locking to the cortical slow oscillation cycles (Supplementary Fig. 2).

Discussion

The present study provides a precise analysis of LC temporal relations to slow oscillations in the nonanaesthetized state, during natural sleep. Additional phase analysis clearly establishes that there is almost no overlap in the preferred phase-of-firing of mPFC and LC neurons relative to the slow oscillation cycle (Figs 3 and 4). A population of LC neurons (52%), time locked to the slow oscillation cycles, fires during the rising edge of the EEG slow wave (previously shown to correlate with transition from Down-to-Up state), while mPFC neurons fire later, namely around the peak of the slow wave. This presumably corresponds to the time of maximal cortical excitability during Up states. Thus, in the chain of the events leading to cortical depolarized states, LC neurons fire before mPFC. This result rules out the possibility that LC firing is caused by prefrontal descending input during Up state. It rather suggests that in prefrontal–coerulear interactions, LC leads mPFC activity.

Phase analysis of the firing of mPFC neurons as a function of the slow oscillation cycle confirmed several previous reports that cortical neurons fire during the Up state (Mölle et al. 2006; Volgushev et al. 2006; Luczak et al. 2007; Peyrache, Benchenane, et al. 2009; Chauvette et al. 2010). Furthermore, there is minimal overlap in the preferred phase-of-firing of mPFC and LC neurons relative to the slow oscillation cycle (Figs 3 and 4). This sheds some light on our early observation in anesthetized rats that showed anticorrelated temporal firing pattern for prefrontal and LC neurons with LC neurons firing in between the cortical bursts (Sara and Herve-Minvielle 1995, see Fig. 4). This phasic opposition was seen, if and only if both regions were in a slow oscillation mode (Lestienne et al. 1997).

The strength of locking to the EEG slow oscillations is comparable in the 2 brain regions. However, mPFC and LC neurons are maximally locked to the slow oscillation at different temporal shifts, reflecting different relations between the neuronal activity in each region, and the global EEG signal. Prefrontal spikes are maximally locked to the slow oscillation shifted approximately 100 ms back in time. This observation implies that prefrontal firing contributes maximally to the part of the slow oscillation around its positive peak, which corresponds to cortical Up state. LC spikes are maximally locked to the slow oscillation shifted approximately 50 ms back in time: This result suggests that the LC-NE system contributes to the Down-to-Up state transition. Overall, the fact that LC activity is so closely related to spontaneous fluctuations of cortical excitability implies a functional prefrontal–coerulear interaction during NREM sleep. The relative temporal order of firing of LC and mPFC neurons, together with the evidence for LC firing on the ascending edge of the EEG slow wave, suggests that LC may well be involved in promoting or facilitating Down-to-Up state transitions.

Prefrontal–coerulear interaction can be supported by the reciprocal monosynaptic pathways between the mPFC and LC, revealed through functional and anatomical studies in rats (Luppi et al. 1995; Sara and Herve-Minvielle 1995; Jodo et al. 1998). NE has complex excitatory and inhibitory effects on cortical cells, depending on concentration of the NE and on receptor distribution and affinity in the target region (McCormick et al. 1991). γ-aminobutyric acidergic neurons are also modulated by NE, with subsequent impact on firing of the cortical pyramidal cells (McCormick and Wang 1991). LC heavily innervates thalamic nuclei where NE depolarizes thalamocortical relay cells and causes an increase in their single-spike discharges (McCormick 1989). Finally, most important to our study, NE strongly affects the intrinsic excitability of cells by depolarizing the membrane potential (McCormick et al. 1991). Synchronized depolarizing of the membrane of a large number of cells is characteristic of the depolarized state (Steriade et al. 1993a, 1993b), with the activity spreading from a small number of particularly excitable cells to the rest of the cortical network (Sanchez-Vives and McCormick 2000; Volgushev et al. 2006; Luczak et al. 2007; Peyrache, Benchenane, et al. 2009; Chauvette et al. 2010). Thus, LC firing at the critical time window may facilitate the transition of less excitable cells to an active mode and thus result in recruiting more cells into the functional network. Cortical efferents could, in turn, influence LC activity via direct projections to the LC from mPFC or via indirect pathways (Luppi et al. 1995). The frontal cortex provides both excitatory and inhibitory influences on LC neurons (Sara and Herve-Minvielle 1995; Jodo et al. 1998), although only a small population of neurons in the prefrontal region (~8%) are antidromically driven by stimulation of the LC (Sara and Herve-Minvielle 1995). This frontal influence on LC may contribute to the synchrony during slow oscillations and could account for the fact that only 50% of LC neurons were phase locked to the cortical oscillation. Moreover, other regions may contribute directly or indirectly to the locking of LC neurons to the PFC oscillation, but this remains to be explored.

The tight temporal relation between fluctuations in cortical excitability state and LC activity can be viewed in the light of electrophysiological studies suggesting that slow oscillations synchronize not only cortical activity but also a number of subcortical structures, particularly the thalamus and the hippocampus (Steriade, Contreras, et al. 1993; Timofeev and Steriade 1996; Isomura et al. 2006). Other neuromodulatory nuclei also show synchrony with cortical slow oscillations.

Under anesthesia-induced slow oscillations, cholinergic cells of the pedunculopontine tegmental nucleus (Balatoni and Detari 2003; Mena-Segovia et al. 2008) and putative cholinergic cells of the basal forebrain (Nunez 1996) fire during the cortical Up state. LFPs in the ventral tegmental area (VTA) show high coherence with slow oscillations in PFC, with peaks in PFC slightly preceding those in VTA, leading the authors to suggest that PFC may be driving VTA, while dopamine input from VTA may act to sustain the cortical Up state (Peters et al. 2004). The results of electrophysiological studies have been corroborated by a recent combined EEG and fMRI study in humans revealing significant blood oxygen level–dependent responses associated with slow oscillations in several brain regions including midbrain and brain stem cholinergic and aminergic nuclei, especially LC (Dang-Vu et al. 2008). Thus, slow oscillations provide a mechanism for a coordinated activity of distant and, possibly, functionally connected neuronal populations. It is evident from all these studies that different neuronal populations have different phase preferences relative to the slow oscillation cycle, possibly reflecting the specific nature of the cross-region interaction. The present study clearly demonstrates in naturally sleeping rats that LC neurons consistently fire at a critical time at the Down-to-Up state transition.

The functional significance can be appreciated within the context of sleep-mediated memory consolidation. The cortical slow oscillations are thought to temporally coordinate the neural activity in other brain areas and thus facilitate interregional communication (Buzsaki 1996). Slow oscillations tend to group delta waves and sleep spindles (Steriade et al. 1993a, 1993b; Mölle et al. 2002, 2006). The sharp wave/ripple complexes recorded in hippocampus are likewise grouped by slow oscillations (Sirota et al. 2003; Battaglia et al. 2004; Mölle et al. 2006). It is during these large-scale high-frequency events that ensembles of neurons "replay" the experience-induced patterns (Kudrimoti et al. 1999; Nadasdy et al. 1999; Ji and Wilson 2007; Peyrache, Khamassi, et al. 2009; Johnson et al. 2010). These authors and others concur that the function of this neuronal replay is to enhance plasticity within and between brain regions, thereby promoting memory consolidation (Buzsaki 1996; Steriade and Timofeev 2003; Steriade 2006). A recent study by Peyrache et al. (2009) shows that "reactivation strength," or replay, is greater after learning a new rule in a prefrontal-dependent task. The patterns of activity that contributed most to the replay in mPFC after acquisition of a new rule were those that were activated at the choice point in the maze. LC neurons may be recruited at the same time, as a part of the extended cortico-hippocampal network encoding new information. This notion is supported by the fact that LC neurons display robust task-related firing: 1) when an animal is engaged in goal-directed behavior, 2) is presented with salient stimuli, or 3) anticipates reward (Bouret and Sara 2004, 2005; Aston-Jones and Cohen 2005).

We have recently shown that LC neurons exhibit a learning-dependent transient activation during NREM sleep (Eschenko and Sara 2008). If the LC-NE system is, indeed, part of the functional learning-associated network, then release of NE contemporaneously with the reactivation of cortico-hippocampal ensembles will serve to reinforce the synaptic plasticity in a selected subpopulation of neurons. It has been known for a long time that NE has a facilitative and even a permissive effect on synaptic plasticity within the hippocampus (Neuman and Harley 1983; Kitchigina et al. 1997), and recent work shows similar effects within the mPFC (Marzo et al. 2009). Moreover, a recent study shows that electrical stimulation of LC enhances and prolongs the long-term potentiation of hippocampal–prefrontal synapses induced by high-frequency stimulation of hippocampus (Lim et al. 2010). This demonstration of facilitation of synaptic plasticity between the 2 brain regions by activation of the LC, together with the present results indicating that activation of the LC-NE system occurs at the times of the cortico-hippocampal neuronal replay, suggests a novel and intriguing role for the LC in sleep-dependent memory consolidation.

Funding

NRJ Fondation de France (to S.J.S.); CNRS PICS (to S.J.S. and O.E.); BMI project of the Italian Institute of Technology (to S.P.).

Supplementary Material

Supplementary material can be found at: http://www.cercor.oxfordjournals.org/

Notes

Conflict of Interest: None declared.

References

Aston-Jones G, Bloom FE. 1981. Activity of norepinephrine-containing locus coeruleus neurons in behaving rats anticipates fluctuations in the sleep-waking cycle. J Neurosci. 1:876–886.

Aston-Jones G, Cohen JD. 2005. An integrative theory of locus coeruleus-norepinephrine function: adaptive gain and optimal performance. Annu Rev Neurosci. 28:403–450.

Axmacher N, Elger CE, Fell J. 2008. Ripples in the medial temporal lobe are relevant for human memory consolidation. Brain. 131:1806–1817.

Balatoni B, Detari L. 2003. EEG related neuronal activity in the pedunculopontine tegmental nucleus of urethane anaesthetized rats. Brain Res. 959:304–311.

Battaglia FP, Sutherland GR, McNaughton BL. 2004. Hippocampal sharp wave bursts coincide with neocortical "up-state" transitions. Learn Memory. 11:697–704.

Bouret S, Sara SJ. 2002. Locus coeruleus activation modulates firing rate and temporal organization of odour-induced single-cell responses in rat piriform cortex. Eur J Neurosci. 16:2371–2382.

Bouret S, Sara SJ. 2004. Reward expectation, orientation of attention and locus coeruleus-medial frontal cortex interplay during learning. Eur J Neurosci. 20:791–802.

Bouret S, Sara SJ. 2005. Network reset: a simplified overarching theory of locus coeruleus noradrenaline function. Trends Neurosci. 28:574–582.

Buzsaki G. 1996. The hippocampo-neocortical dialogue. Cereb Cortex. 6:81–92.

Chauvette S, Volgushev M, Timofeev I. 2010. Origin of active states in local neocortical networks during slow sleep oscillation. Cereb Cortex. 20:2660–2674.

Clemens Z, Fabo D, Halasz P. 2006. Twenty-four hours retention of visuospatial memory correlates with the number of parietal sleep spindles. Neurosci Lett. 403:52–56.

Dang-Vu TT, Schabus M, Desseilles M, Albouy G, Boly M, Darsaud A, Gais S, Rauchs G, Sterpenich V, Vandewalle G, et al. 2008. Spontaneous neural activity during human slow wave sleep. Proc Natl Acad Sci U S A. 105:15160–15165.

Diekelmann S, Born J. 2010. The memory function of sleep. Nat Rev Neurosci. 11:114–126.

Eschenko O, Molle M, Born J, Sara SJ. 2006. Elevated sleep spindle density after learning or after retrieval in rats. J Neurosci. 26:12914–12920.

Eschenko O, Ramadan W, Molle M, Born J, Sara SJ. 2008. Sustained increase in hippocampal sharp-wave ripple activity during slow-wave sleep after learning. Learn Mem. 15:222–228.
Eschenko O, Sara SJ. 2008. Learning-dependent, transient increase of activity in noradrenergic neurons of locus coeruleus during slow wave sleep in the rat: brain stem-cortex interplay for memory consolidation? Cereb Cortex. 18:2596–2603.
Fisher NI. 1993. Statistical analysis of circular data. Cambridge: Cambridge University Press.
Fogel SM, Smith CT. 2006. Learning-dependent changes in sleep spindles and Stage 2 sleep. J Sleep Res. 15:250–255.
Foote SL, Aston-Jones G, Bloom FE. 1980. Impulse activity of locus coeruleus neurons in awake rats and monkeys is a function of sensory stimulation and arousal. Proc Natl Acad Sci U S A. 77:3033–3037.
Gais S, Molle M, Helms K, Born J. 2002. Learning-dependent increases in sleep spindle density. J Neurosci. 22:6830–6834.
Harley CW. 2007. Norepinephrine and the dentate gyrus. Prog Brain Res. 163:299–318.
Herve-Minvielle A, Sara SJ. 1995. Rapid habituation of auditory responses of locus coeruleus cells in anaesthetized and awake rats. Neuroreport. 6:1363–1368.
Hobson JA, McCarley RW, Wyzinski PW. 1975. Sleep cycle oscillation: reciprocal discharge by two brainstem neuronal groups. Science. 189:55–58.
Isomura Y, Sirota A, Ozen S, Montgomery S, Mizuseki K, Henze DA, Buzsaki G. 2006. Integration and segregation of activity in entorhinal-hippocampal subregions by neocortical slow oscillations. Neuron. 52:871–882.
Ji D, Wilson MA. 2007. Coordinated memory replay in the visual cortex and hippocampus during sleep. Nat Neurosci. 10:100–107.
Jodo E, Chiang C, Aston-Jones G. 1998. Potent excitatory influence of prefrontal cortex activity on noradrenergic locus coeruleus neurons. Neuroscience. 83:63–79.
Johnson LA, Euston DR, Tatsuno M, McNaughton BL. 2010. Stored-trace reactivation in rat prefrontal cortex is correlated with down-to-up state fluctuation density. J Neurosci. 30:2650–2661.
Kitchigina V, Vankov A, Harley C, Sara SJ. 1997. Novelty-elicited, noradrenaline-dependent enhancement of excitability in the dentate gyrus. Eur J Neurosci. 9:41–47.
Kudrimoti HS, Barnes CA, McNaughton BL. 1999. Reactivation of hippocampal cell assemblies: effects of behavioral state, experience, and EEG dynamics. J Neurosci. 19:4090–4101.
Lestienne R, Herve-Minvielle A, Robinson D, Briois L, Sara SJ. 1997. Slow oscillations as a probe of the dynamics of the locus coeruleus-frontal cortex interaction in anesthetized rats. J Physiol Paris. 91:273–284.
Lim EP, Tan CH, Jay TM, Dawe GS. 2010. Locus coeruleus stimulation and noradrenergic modulation of hippocampo-prefrontal cortex long-term potentiation. Int J Neuropsychopharmacol. 13(9):1219–1231.
Luczak A, Bartho P, Marguet SL, Buzsaki G, Harris KD. 2007. Sequential structure of neocortical spontaneous activity in vivo. Proc Natl Acad Sci U S A. 104:347–352.
Luppi PH, Aston-Jones G, Akaoka H, Chouvet G, Jouvet M. 1995. Afferent projections to the rat locus coeruleus demonstrated by retrograde and anterograde tracing with cholera-toxin B subunit and Phaseolus vulgaris leucoagglutinin. Neuroscience. 65:119–160.
Marzo A, Bai J, Otani S. 2009. Neuroplasticity regulation by noradrenaline in mammalian brain. Curr Neuropharmacol. 7:286–295.
McCormick DA. 1989. Cholinergic and noradrenergic modulation of thalamocortical processing. Trends Neurosci. 12:215–221.
McCormick DA, Pape HC, Williamson A. 1991. Actions of norepinephrine in the cerebral cortex and thalamus: implications for function of the central noradrenergic system. Prog Brain Res. 88:293–305.
McCormick DA, Wang Z. 1991. Serotonin and noradrenaline excite GABAergic neurones of the guinea-pig and cat nucleus reticularis thalami. J Physiol. 442:235–255.
Mena-Segovia J, Sims HM, Magill PJ, Bolam JP. 2008. Cholinergic brainstem neurons modulate cortical gamma activity during slow oscillations. J Physiol. 586:2947–2960.
Mölle M, Marshall L, Gais S, Born J. 2002. Grouping of spindle activity during slow oscillations in human non-rapid eye movement sleep. J Neurosci. 22:10941–10947.
Mölle M, Yeshenko O, Marshall L, Sara SJ, Born J. 2006. Hippocampal sharp wave-ripples linked to slow oscillations in rat slow-wave sleep. J Neurophysiol. 96:62–70.
Montemurro MA, Rasch MJ, Murayama Y, Logothetis NK, Panzeri S. 2008. Phase-of-firing coding of natural visual stimuli in primary visual cortex. Curr Biol. 18:375–380.
Morin A, Doyon J, Dostie V, Barakat M, Hadj Tahar A, Korman M, Benali H, Karni A, Ungerleider LG, Carrier J. 2008. Motor sequence learning increases sleep spindles and fast frequencies in post-training sleep. Sleep. 31:1149–1156.
Nadasdy Z, Hirase H, Czurko A, Csicsvari J, Buzsaki G. 1999. Replay and time compression of recurring spike sequences in the hippocampus. J Neurosci. 19:9497–9507.
Neuman RS, Harley CW. 1983. Long-lasting potentiation of the dentate gyrus population spike by norepinephrine. Brain Res. 273:162–165.
Nunez A. 1996. Unit activity of rat basal forebrain neurons: relationship to cortical activity. Neuroscience. 72:757–766.
O'Neill J, Senior TJ, Allen K, Huxter JR, Csicsvari J. 2008. Reactivation of experience-dependent cell assembly patterns in the hippocampus. Nat Neurosci. 11:209–215.
Peters Y, Barnhardt NE, O'Donnell P. 2004. Prefrontal cortical up states are synchronized with ventral tegmental area activity. Synapse. 52:143–152.
Peyrache A, Benchenane K, Khamassi M, Wiener SI, Battaglia FP. 2009. Sequential reinstatement of neocortical activity during slow oscillations depends on cells' global activity. Front Syst Neurosci. 3.doi: 10.3389/neuro.3306.3018.2009.
Peyrache A, Khamassi M, Benchenane K, Wiener SI, Battaglia FP. 2009. Replay of rule-learning related neural patterns in the prefrontal cortex during sleep. Nat Neurosci. 12:919–926.
Ramadan W, Eschenko O, Sara SJ. 2009. Hippocampal sharp wave/ripples during sleep for consolidation of associative memory. PLoS One. 4:e6697.
Roullet P, Sara S. 1998. Consolidation of memory after its reactivation: involvement of beta noradrenergic receptors in the late phase. Neural Plast. 6:63–68.
Saleem AB, Chadderton P, Apergis-Schoute J, Harris KD, Schultz SR. 2010. Methods for predicting cortical UP and DOWN states from the phase of deep layer local field potentials. J Comput Neurosci. 29:49–62.
Sanchez-Vives MV, McCormick DA. 2000. Cellular and network mechanisms of rhythmic recurrent activity in neocortex. Nat Neurosci. 3:1027–1034.
Sara SJ, Herve-Minvielle A. 1995. Inhibitory influence of frontal cortex on locus coeruleus neurons. Proc Natl Acad Sci U S A. 92:6032–6036.
Sara SJ, Segal M. 1991. Plasticity of sensory responses of locus coeruleus neurons in the behaving rat: implications for cognition. Prog Brain Res. 88:571–585.
Schabus M, Gruber G, Parapatics S, Sauter C, Klosch G, Anderer P, Klimesch W, Saletu B, Zeitlhofer J. 2004. Sleep spindles and their significance for declarative memory consolidation. Sleep. 27:1479–1485.
Siapas AG, Lubenov EV, Wilson MA. 2005. Prefrontal phase locking to hippocampal theta oscillations. Neuron. 46:141–151.
Siapas AG, Wilson MA. 1998. Coordinated interactions between hippocampal ripples and cortical spindles during slow-wave sleep. Neuron. 21:1123–1128.
Sirota A, Csicsvari J, Buhl D, Buzsaki G. 2003. Communication between neocortex and hippocampus during sleep in rodents. Proc Natl Acad Sci U S A. 100:2065–2069.
Steriade M. 2006. Grouping of brain rhythms in corticothalamic systems. Neuroscience. 137:1087–1106.
Steriade M, Contreras D, Curro Dossi R, Nunez A. 1993. The slow (<1 Hz) oscillation in reticular thalamic and thalamocortical neurons: scenario of sleep rhythm generation in interacting thalamic and neocortical networks. J Neurosci. 13:3284–3299.

Steriade M, Nunez A, Amzica F. 1993a. Intracellular analysis of relations between the slow (<1 Hz) neocortical oscillation and other sleep rhythms of the electroencephalogram. J Neurosci. 13:3266–3283.
Steriade M, Nunez A, Amzica F. 1993b. A novel slow (<1 Hz) oscillation of neocortical neurons in vivo: depolarizing and hyperpolarizing components. J Neurosci. 13:3252–3265.
Steriade M, Timofeev I. 2003. Neuronal plasticity in thalamocortical networks during sleep and waking oscillations. Neuron. 37:563–576.
Steriade M, Timofeev I, Grenier F. 2001. Natural waking and sleep states: a view from inside neocortical neurons. J Neurophysiol. 85:1969–1985.
Stickgold R. 2005. Sleep-dependent memory consolidation. Nature. 437:1272–1278.
Timofeev I, Grenier F, Steriade M. 2001. Disfacilitation and active inhibition in the neocortex during the natural sleep-wake cycle: an intracellular study. Proc Natl Acad Sci U S A. 98:1924–1929.
Timofeev I, Steriade M. 1996. Low-frequency rhythms in the thalamus of intact-cortex and decorticated cats. J Neurophysiol. 76:4152–4168.
Tronel S, Feenstra MG, Sara SJ. 2004. Noradrenergic action in prefrontal cortex in the late stage of memory consolidation. Learn Mem. 11:453–458.
Volgushev M, Chauvette S, Mukovski M, Timofeev I. 2006. Precise long-range synchronization of activity and silence in neocortical neurons during slow-wave oscillations [corrected]. J Neurosci. 26:5665–5672.